Environmental Science Processes & Impacts

ROYAL SOCIETY OF CHEMISTRY

PAPER

View Article Online
View Journal | View Issue

Cite this: *Environ. Sci.: Processes Impacts*, 2026, **28**, 763

Mechanisms of ozone effects on plant stress in soybean across growing season: from leaf to regional perspective

Luka Mamić, *[abc] Mj Riches, [bd] Rose K. Rossell [b] and Delphine K. Farmer *[b]

Ground-level ozone (O_3) is a major constraint on agricultural productivity, yet most knowledge comes from controlled fumigation experiments using chronic exposures that differ from the episodic conditions crops experience in the field. Here, we combine a five-week chamber experiment with multi-year satellite observations (2018–2021, Arkansas, U.S.) to investigate how O_3 affects photosynthesis, efficiency, and growth across scales of soybean plants (*Glycine max*). At the leaf level, initial O_3 fumigation (80 ppb for 4 h) caused the strongest suppression of CO_2 assimilation (A), stomatal conductance (G_s), and photosystem II efficiency (Φ_{PSII}), indicating entry into a physiological strain phase. Recovery between exposures was incomplete, leading to sustained growth reductions despite moderate O_3 levels. At the regional scale, analysis of solar-induced fluorescence (SIF) and MODIS productivity metrics revealed parallel patterns. Early-season O_3 episodes produced greater suppression of SIF, GPP, and G_s compared to equivalent late-season events, and recovery lagged for several weeks. Seasonal yield proxies were best explained not by total O_3 accumulation, but by early- and peak-season exposures, which accounted for up to 98% of variance across four growing seasons. Our findings highlight that the timing of O_3 episodes is more consequential than cumulative dose, and that functional indicators such as SIF can detect strain-phase stress before structural indices diverge. By linking controlled experiments with regional-scale satellite monitoring, this study advances mechanistic understanding of O_3 impacts on soybean and supports the development of remote sensing-based early warning tools for crop management.

Received 26th September 2025
Accepted 30th January 2026

DOI: 10.1039/d5em00785b

rsc.li/espi

Environmental significance

Ground-level ozone (O_3) is a pervasive air pollutant that threatens food security, but most risk assessments are based on chronic, elevated exposures that poorly represent real agroecosystems. By linking controlled fumigation experiments with multi-year satellite observations, this study shows that the timing of O_3 exposure, particularly during early and peak growth stages, is more damaging to soybean productivity than total seasonal dose. Even moderate, short-term O_3 episodes, under current regulations, suppressed photosynthesis, slowed canopy development, and reduced yield proxies under otherwise healthy field conditions. We further demonstrate that solar-induced chlorophyll fluorescence can detect O_3 stress before visible damage occurs, offering a scalable tool for monitoring crop vulnerability.

1. Introduction

Air pollution threatens agricultural productivity and food security around the globe.[1,2] Among air pollutants, ground-level ozone (O_3) is one of the most important stressors to global crop production.[3,4] O_3 is a secondary air pollutant formed *via* photochemical reactions between nitrogen oxides and volatile organic compounds. The terrestrial biosphere is a key sink for O_3, which may reduce atmospheric concentrations of this pollutant, but means that O_3 deposition can directly impact crop yield and productivity.[5,6] Even short-term periods of elevated O_3 can significantly decrease yields,[2,7] with soybean being one of the most sensitive – yet economically important – crops.[8,9]

While there is a broad understanding of O_3-plant interactions, many details remain unclear, such as species-specific physiological responses,[10] the mechanisms underlying photosynthetic and metabolic impairments,[11] and interactions with climatic and agronomic factors.[12] Plants primarily regulate O_3 entry through stomatal control, yet stomatal uptake accounts

[a]*Department of Civil, Building and Environmental Engineering, Sapienza University of Rome, Via Eudossiana 18, 00184, Rome, Italy. E-mail: luka.mamic@uniroma1.it*
[b]*Department of Chemistry, Colorado State University, 1301 Center Ave Mall, 80523-1872, Fort Collins, Colorado, USA. E-mail: delphine.farmer@colostate.edu*
[c]*Interdepartmental Research Centre in Geomatics (CIRGEO), University of Padua, Corte Benedettina - Via Roma 34, 35020, Legnaro, Italy*
[d]*Department of Agricultural Biology, Colorado State University, 307 University Ave, 80523-1101, Fort Collins, Colorado, USA*

for only ~45% of total ecosystem-level O_3 deposition, with the remainder occurring *via* non-stomatal pathways such as uptake by cuticular surfaces, soil, and wet leaf films.[5] These non-stomatal routes are especially important in dry conditions when stomata are partially closed, as harmful oxidative stress may persist internally,[13] eventually impairing photosynthesis and accelerating senescence which leads to yield losses in sensitive crops.[9,14] Felzer *et al.*[15] used a coupled biosphere-atmosphere model to estimate that, under extreme conditions, surface O_3 could reduce global crop yields by up to 20% for wheat and 60% for soybeans by 2100. These reductions stem from the chronic suppression of photosynthesis and biomass accumulation based on dose–response functions from chamber and field experiments built into their model. When these losses were integrated over time and scaled to global agricultural output, the cumulative economic loss was estimated to be up to $8 trillion. This loss would primarily affect major food-producing regions in North America and Asia. Despite recognition of this scale, most large-scale estimates still rely on simplified exposure-response functions,[12,16–19] while the mechanistic pathways of O_3 damage across growth stages and environments remain poorly resolved. In particular, little is known about how repeated, realistic O_3 exposures interact with climatic variability to shape the transition from hidden physiological strain to visible damage and yield loss.

Plant stress can be generally described by three successive phases: (i) an initial state of applied force, (ii) a strain phase in which stress is expressed before visible damage occurs, and (iii) the damage phase, in which acute and chronic injury become visible on the leaf surface.[20] These phases are particularly challenging to study under O_3 exposure because they require carefully controlled fumigation with a highly reactive and toxic gas. Many experiments have relied on either a single acute pulse of unrealistically high O_3 (ref. 21 and 22) or long-term chronic exposures.[9,23] In contrast, O_3 in the field fluctuates with the diurnal cycle and is punctuated by episodic high-O_3 days.[5,24] The physiological effects of repeated exposures to realistic, fluctuating concentrations may therefore differ substantially from those observed under strictly acute or chronic treatments.

Soybean, the second most widely grown crop in the United States (U.S.) and a supplier of more than one-third of global production,[28] is highly susceptible to elevated O_3, which significantly reduces photosynthesis, stomatal conductance (G_s), biomass accumulation, and seed yield.[8,9,21] Meta-analyses report average shoot biomass reductions of up to 34% and yield reductions of ~24% under chronic exposures near 70 parts per billion by volume (ppb) O_3.[9] The main physiological processes affected by O_3 include carboxylation efficiency (the capacity to fix CO_2 during photosynthesis), photosystem II efficiency (Φ_{PSII}, the effectiveness of light-driven electron transport), and carbon allocation patterns (the distribution of assimilated carbon between growth and storage).[8,22] Variations among cultivars and climatic conditions further complicate these responses.[23]

At the field scale, the SoyFACE (Soybean Free Air Concentration Enrichment) project provided critical evidence on the effects of chronic O_3 under open-air, agronomic conditions. Experiments at SoyFACE demonstrated significant reductions in canopy photosynthesis, earlier leaf senescence, and lower harvest index values in soybeans exposed to elevated O_3 (~60–70 ppb average daytime concentration, sustained across full growing seasons).[16,17,25–27] These physiological effects were often undetectable with canopy greenness-based indices such as the normalized difference vegetation index (NDVI), which primarily captures structural leaf area and chlorophyll content. By contrast, solar-induced chlorophyll fluorescence (SIF), a direct proxy for photochemical efficiency, and gas exchange measurements of photosynthesis and G_s provide more sensitive indicators of early stress. Using these approaches, SoyFACE studies identified the strain phase of O_3 stress.[26] Furthermore, SoyFACE results confirmed reproductive growth stages are especially vulnerable, showing reduced maximum rate of carboxylation (V_{cmax}), maximum rate of electron transport (J_{max}), and faster canopy decline under elevated O_3 conditions.[25] While SoyFACE and similar experiments provide key insight into soybean responses, they simulated future chronic air quality scenarios by maintaining elevated O_3 for entire growing seasons. In contrast, agricultural ecosystems today are often exposed to O_3 in shorter, episodic bursts, such as a few hours on high-O_3 afternoons, or multiple exceedance events across a season depending on location.[28–30] Defining what constitutes "high O_3" in agronomic terms, and understanding how repeated realistic exposures differ from strictly acute or strictly chronic treatments, remains an unresolved challenge. These differences are critical for establishing thresholds for O_3 damage in soybean[12,17] and for clarifying the mechanisms by which plants defend against and recover from varying O_3 stress regimes.[22,23]

Remote sensing offers a useful pathway to investigate these knowledge gaps across agroecosystems. However, traditional remote sensing indices (*e.g.*, NDVI) can only detect the damage phase of stress after visible morphological changes have occurred.[31,32] At that stage, damage is often irreversible, as photosynthetic machinery and leaf area are already degraded and yield potential cannot be recovered.[9,25] However, if the stressor is removed during the strain phase, the plant can partially recover and reestablish a new physiological standard.[20] SIF is a promising parameter for detecting the strain phase earlier. Ground-based SIF measurements can monitor photosynthetic efficiency before visible symptoms develop.[26] Recently-available satellite SIF data from, for example, the TROPOspheric Monitoring Instrument (TROPOMI) onboard Sentinel-5P, provides an opportunity to identify crop stress across larger scales and in near-real time. Such analyses, however, require a mechanistic understanding of how crop fluorescence responds to O_3 exposure.

This study addresses how repeated, realistic O_3 exposures interact with environmental conditions to affect soybean physiology, and the need to evaluate when and how such stress becomes detectable with remote sensing. We combine a five-week plant-level exposure experiment with multi-year satellite observations of soybean fields in Arkansas, U.S. (2018–2021) to investigate O_3 stress across spatial and temporal scales. Specifically, we aim to (i) identify the strain phase of O_3 stress,

when physiological impairment occurs before visible damage; (ii) determine when during the growing season O_3 stress is most consequential for soybean development; (iii) assess the potential for recovery following episodic O_3 exposure and how this differs between controlled and field conditions; and (iv) evaluate the capacity of remote sensing indicators, particularly SIF, to detect these processes at regional scale. By integrating experimental and remote sensing perspectives, our goal is to improve mechanistic understanding of O_3 stress in soybean and contribute to the development of remote sensing-based early warning systems and decision-support tools for farmers and agronomists.

2. Methodology

Our study integrates experiments and observations across spatial and temporal scales. We began with controlled, leaf-level measurements using a portable photosynthesis system (PPS) and extended the analysis to regional-scale using satellite remote sensing data. Conditions in the chamber experiment were designed to replicate the average temperature and relative humidity (RH) observed over four soybean growing seasons (2018–2021) in Crittenden County, Arkansas (Section 2.2) (Fig. S1). The same environmental settings were applied during PPS measurements (Section 2.1) to ensure consistency across scales. This approach allowed us to compare chamber findings with multi-year satellite observations from TROPOMI and the Moderate Resolution Imaging Spectroradiometer (MODIS).

We emphasize that chamber and satellite results are not directly comparable because they represent very different spatial scales (leaf *vs.* field). Instead, our aim was to test whether the mechanisms of O_3 stress observed under controlled conditions also emerge at the regional scale, linking mechanistic understanding with applied monitoring. Based on the remote sensing data, soybean fields in Crittenden County did not experience numerous extreme weather or pollution events during the observed period (Fig. S1 and S2), representing relatively healthy agroecosystems – making this study both more challenging and more relevant, as it examines O_3 effects under moderate, yet realistic, conditions.

2.1. Plant-level chamber experiments

Soybeans (*Glycine max*) were grown from seed. Seeds were sown in small containers on 06 February 2025, and germination began on 12 February 2025. Plants grew under controlled laboratory conditions with a standard 12 hours light–dark cycle. Other than during fumigation periods (conducted in a chamber and described below), plants were exposed only to ambient laboratory O_3 levels, with daily means of ~30 ppb.

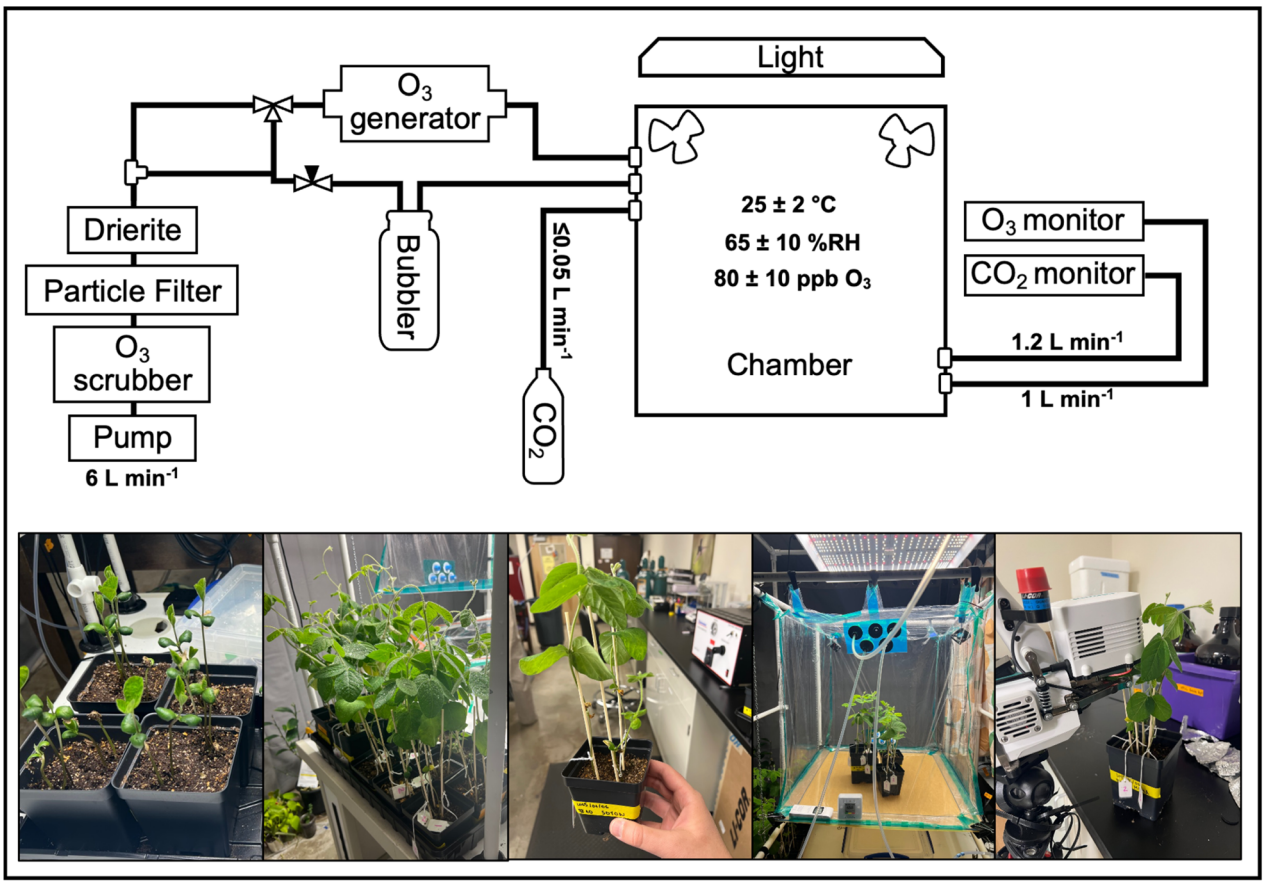

Fig. 1 Schematic of the custom-built plant fumigation chamber (top) and photos from the soybean vegetative growth cycle during the experiment (bottom). Total inlet flow of 6 L min^{-1} was split between the O_3 and humidification lines as needed to regulate RH and O_3.

The fumigation chamber (0.61 m × 0.61 m × 0.61 m) was made of transparent, chemical-resistant, polytetrafluoroethylene film with perfluoroalkoxy and polytetrafluoroethylene Swagelok fittings coupled with clear fluorinated ethylene propylene tubing (Fig. 1). A 60 L food-grade CO_2 cylinder (Sodastream) maintained mixing ratios in the chamber at ~400 ppm. Lab air was pushed by a Gast compressor/vacuum pump (DOA-P704-AA) through a bubbler system with deionized water into the chamber to maintain RH at 65 ± 10% throughout the fumigation. Internal chamber temperature was 25 ± 2 °C. A 300 W LED grow light (MARS HYDRO) controlled light intensity at 1000 μmol m^{-2} s^{-1}, measured at the top of the chamber. A Li-COR CO_2/H_2O gas analyzer (LI-840A) and a 2B-Technologies O_3 monitor (Model 202) continuously measured chamber CO_2 and O_3 mixing ratios.

The five-week plant-level experiment started on 03 March 2025. During this period, 1–3 leaves from each selected plant (five leaves in total) were measured weekly using a Li-Cor LI-6800 PPS. Parameters included CO_2 assimilation (A, rate of CO_2 movement through the stomata) stomatal conductance (G_s, movement of CO_2 and H_2O through the stomata).[33] We also measured maximum light-adapted fluorescence (F_m') and steady-state fluorescence (F_s) which were used to calculate Φ_{PSII}. PPS leaf chamber conditions were set to 26 ± 0.2 °C and 63 ± 0.5% RH, equivalent to 1.36 ± 0.04 kPa VPD. These conditions matched the growth chamber environment and were representative of field conditions in Crittenden County, Arkansas (see Section 2.2, Fig. S1).

Plants were divided into two groups: three controls and three O_3 fumigation plants. Both groups followed the same measurement schedule and chamber conditions. Each week, fumigated plants were exposed for four hours to 80 ± 10 ppb O_3 generated by a pen-ray lamp (Analytik Jena AG) connected to the dry air inlet. This exposure corresponds approximately to an 8 hours mean O_3 concentration of ~40 ppb, which is representative of typical daytime O_3 levels observed during the soybean growing season (Fig. S2). PPS measurements were taken on five leaves immediately before each exposure (pre-treatment) following a 20 minutes acclimation period, and again immediately after exposure (post-treatment). These measurements were taken immediately before and after weekly O_3 exposure in the fumigation chamber; plants were otherwise continuously maintained under identical laboratory conditions. Control plants underwent the same procedure, but without O_3 fumigation. This cycle was repeated weekly for five consecutive weeks, during which plants advanced through vegetative growth and began pod development (Fig. 1). The five-week chamber experiment spans early vegetative development and is designed to probe physiological responses to initial and repeated episodic O_3 exposure, rather than to represent the full seasonal progression of soybean growth.

Being aware of the limited leaf-level dataset and the importance of distinguishing biological outliers from systematic ones,[34,35] we applied the stricter approach of Leys *et al.*,[36] excluding values outside three median absolute deviations (MADs) (Fig. S3). This approach minimizes the impact of errors in measurements while maintaining the most representative physiological responses. We also note that measurements of *A* in week five may be confounded by plants nearing the end of their life cycle or by limitations to root growth from the small containers.

The results of the chamber experiment are presented in Section 3, including analyses of (i) soybean leaf responses to initial O_3 exposure, (ii) recovery potential between repeated exposures, (iii) effects of fumigation on plant growth, and (iv) the behavior of photosynthetic fluorescence parameters under subtle O_3 stress.

2.2. Remote sensing analysis

The chosen study area, shown on Fig. 2, located in Crittenden County (Arkansas, U.S.), is a significant soybean-producing region in a state that ranks among the top soybean producers nationally.[37] Due to the coarse spatial resolution of the TROPOMI SIF product (7 × 3.5 km), two points of interest were selected over a cluster of large soybean fields (AR1 and AR2).

To evaluate the impact of O_3 on soybean fields at the regional scale, we integrated multiple datasets (Table 1) (Fig. 3 and S4). Ground-level O_3 data from a nearby Environmental Protection Agency (EPA) monitoring station in Crittenden County provided daily 8 hours means and hourly concentrations, the latter used to calculate weekly AOT40 by summing exceedances of O_3 above 40 ppb during daylight hours (08:00 to 20:00). Daily meteorological variables, including maximum temperature (T_{max}), RH, VPD, grass reference evapotranspiration (ETo), and precipitation (PREC) were obtained from the University of Idaho GRIDMET dataset.[38] MODIS datasets provided vegetation and productivity indicators, including 8 days cumulative gross primary production (GPP, the total carbon fixed by plants through photosynthesis summed over 8 days period),[39] 4 days composite fraction of photosynthetically active radiation (fPAR, the portion of incoming sunlight absorbed by the canopy), 4 days composite leaf area index (LAI, one-sided green leaf area per unit ground area), daily NDVI (derived from surface reflectance, as a measure of canopy greenness), and 3-hourly total photosynthetically active radiation (PAR, incident solar radiation in the visible spectrum (400–700 nanometers)).

SIF 743 nm data were derived from the ESA-TROPOSIF project,[40] which uses daily Sentinel-5P TROPOMI measurements. Data from May 2018 to December 2021 were extracted over selected points, filtered to remove negative and extreme values, and averaged between fields to maximize signal coherence. The analysis period covered four soybean growing seasons, each defined as the period from April to September. Within each season, we further subdivided the timeframe into early, peak, and late stages based on SIF dynamics. The peak season range was defined as the four weeks before and after the maximum SIF value. The four weeks prior to the peak period were defined as the early season, and the four weeks after the peak period were defined as the late season, corresponding with senescence and harvesting (Fig. 3).

We aggregated all datasets to a weekly scale for analysis. Weekly water balance (WB) was calculated as the difference

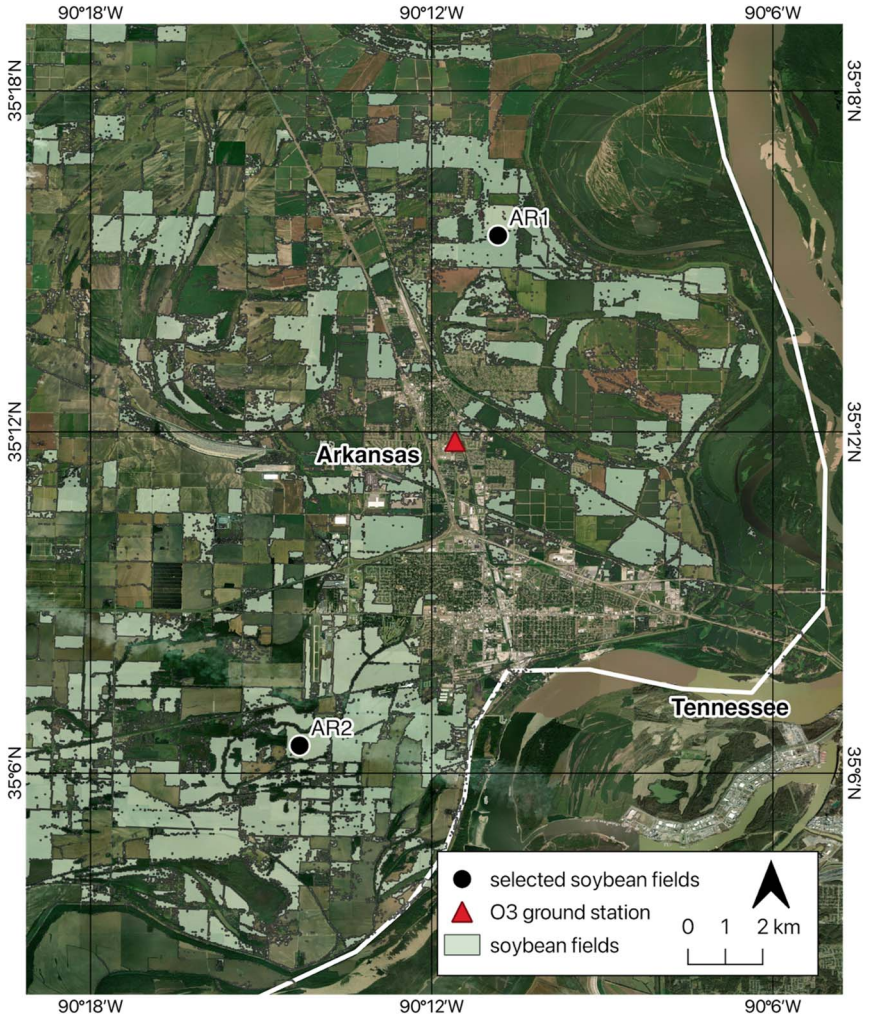

Fig. 2 Study area in Crittenden County, Arkansas, U.S.

between accumulated PREC and ETo. Each of the eight 3-hourly PAR bands per day (in W m^{-2}) was converted to photons using the standard factor for sunlight (1 W m^{-2} ≈ 4.57 μmol m^{-2} s^{-1}) and integrated over 10 800 s (3 hours), summed across the day and then across seven days to obtain weekly incident PAR (mol m^{-2} $weeks^{-1}$).[41,42] 8 day GPP was first divided by 8 to get approximate daily values and then summed across week. We calculated weekly absorbed photosynthetically active radiation (APAR) as APAR = PAR × fPAR, which was used to calculate weekly light use deficiency (LUE) as LUE = GPP/APAR, and

Table 1 Specifications of datasets used in this study for remote sensing analysis

Data	Description	Units	Temporal resolution	Spatial resolution	Source
O_3	*In situ* ozone	ppb	Daily	—	EPA
SIF	Solar-induced fluorescence at 743 nm	mW m^{-2} sr^{-1} nm^{-1}	Daily	7 × 3.5 km	ESA-TROPOSIF
T_{max}	Maximum temperature	°C	Daily	4.6 km	GRIDMET
RH	Relative humidity	%	Daily	4.6 km	GRIDMET
VPD	Vapor pressure deficit	kPa	Daily	4.6 km	GRIDMET
PREC	Precipitation amount	mm	Daily	4.6 km	GRIDMET
ETo	Grass reference evapotranspiration	mm	Daily	4.6 km	GRIDMET
GPP	Gross primary production	kgC m^{-2} 8 $days^{-1}$	8 day	0.3 km	MODIS
PAR	Photosynthetically active radiation	W m^{-2}	3 hour	0.5 km	MODIS
fPAR	Fraction of photosynthetically active radiation	—	4 day	0.5 km	MODIS
LAI	Leaf area index	—	4 day	0.5 km	MODIS
NDVI	Normalized difference vegetation index	—	Daily	0.5 km	MODIS

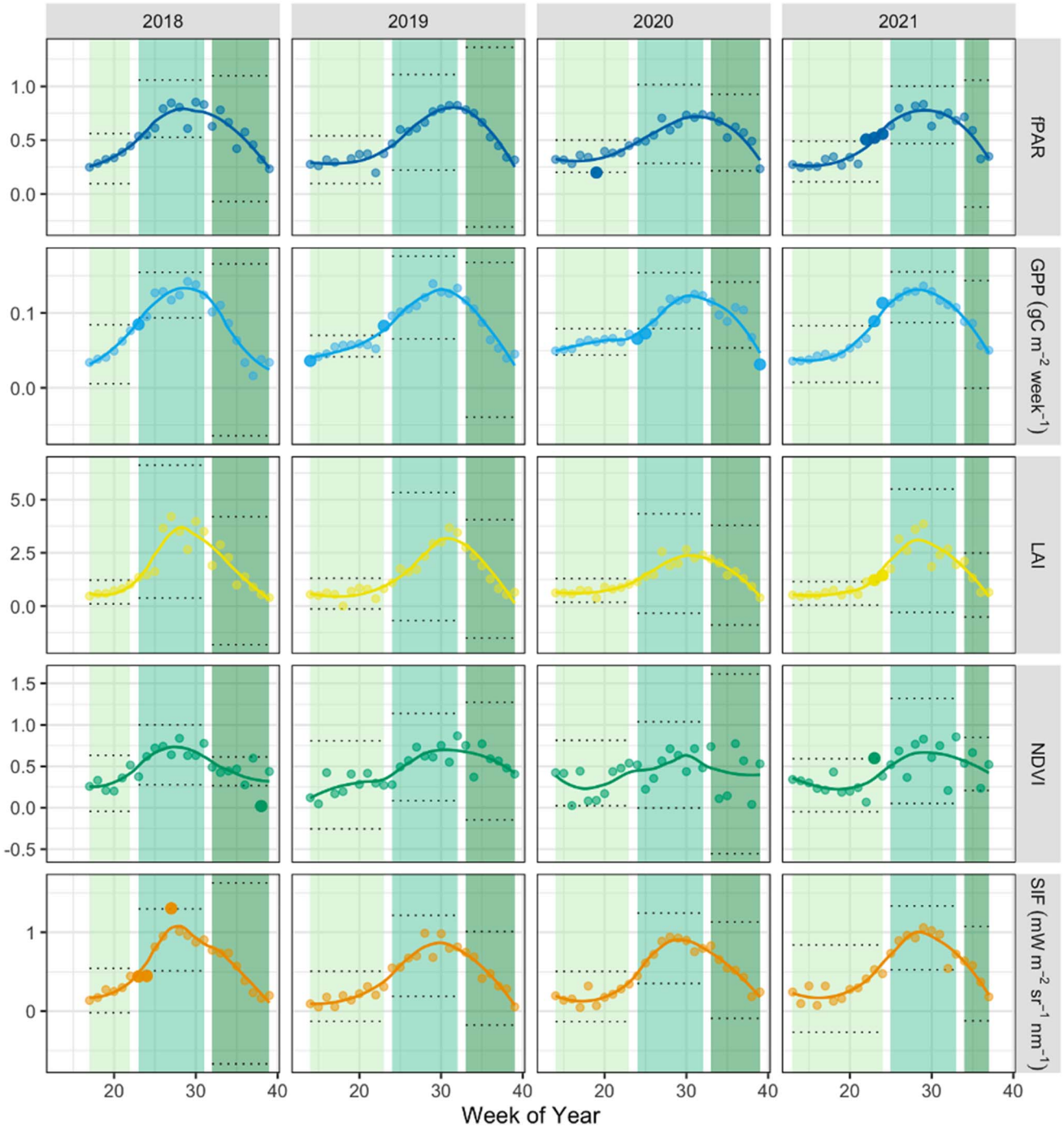

Fig. 3 Weekly time series of vegetation indicators (fPAR, GPP, LAI, NDVI, and SIF) in soybean fields in Crittenden County, Arkansas, across four growing seasons (April–September, 2018–2021). Points show weekly observations, and lines represent smoothed seasonal signatures. Shaded bands indicate the early (light green), peak (mid green), and late (dark green) phases of the growing season. Solid (non-transparent) points mark flagged outliers within each phase.

SIF_{yield} = SIF/APAR (efficiency of energy conversion from absorbed light into fluorescence).[43,44] Following the framework of Massmann *et al.*,[45] we further estimated G_s as a function of GPP and VPD (eqn (1)):

$$G_s \approx \frac{GPP}{\sqrt{VPD}} \quad (1)$$

This proxy eqn (1) assumes that plants open their stomata during photosynthesis (higher GPP) and close them when the atmosphere becomes drier (higher VPD), helping estimate potential O_3 uptake, rather than as a direct measure of stomatal conductance.

The remote sensing allowed us to assess O_3 impacts on soybean physiology at the regional scale across four growing

seasons. In Section 4, we present these results, including analyses of (i) the effects of early *versus* late O_3 episodes, (ii) the potential for recovery in the weeks following O_3 episodes, (iii) the relationship between seasonal O_3 accumulation and yield proxies, and (iv) changes in the coupling between vegetation health indicators under different O_3 conditions. Comparisons with plant-level chamber experiments are made throughout the section to evaluate whether the mechanisms observed at the leaf level can also be detected across larger spatial and temporal scales.

3. Plant-level O_3 fumigation experiment

3.1. Impact of initial O_3 exposure on photosynthesis

Initial exposure (Week 1) to O_3 had the most pronounced immediate effect on all measured physiological parameters (Fig. 4). In the first week of fumigation, treated plants showed a stronger decrease in the ratio of post-to pre-treatment values for both A and G_s compared to controls, indicating early and acute stress response to O_3. This immediate response, which was not observed in following exposures, suggests that plants were not acclimated to the elevated O_3 and had not yet activated defense mechanisms, consistent with earlier reports that initial O_3 events trigger strong physiological reactions in soybean.[9,21] These findings highlight the acute sensitivity of soybean plants during the early vegetative stage and support the idea that timing of exposure is as important as intensity. That is, elevated O_3 early in the growing season is likely to cause more lasting damage on photosynthesis than equivalent exposure later.

In the following weeks, the pattern was reversed: control plants often showed stronger negative post-treatment reactions than fumigated plants. This finding suggests that the chamber environment itself is a stressor, confounding immediate post-fumigation responses and complicating the separation of O_3 effects from chamber effects. Adding O_3 as an additional

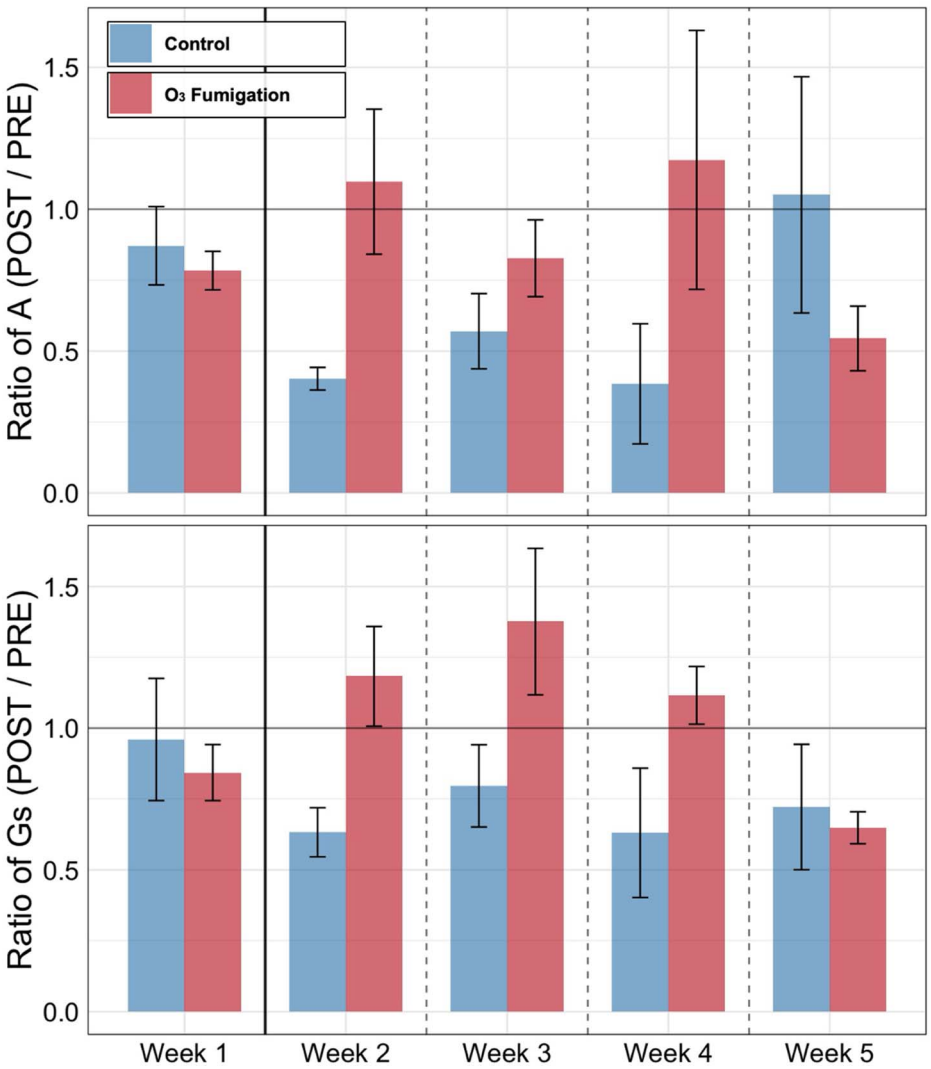

Fig. 4 Physiological responses of soybean plants to O_3 fumigation over five weeks are expressed as the ratio of the post- and pre-treatment measurements of A (top row), and G_s (bottom row). Bars represent the mean ratio ($n = 5$ leaves) ± standard error (SE) for each week of exposure for O_3-treated (red) and control (blue) plants.

stressor may have altered or masked immediate post-fumigation signals, leading to inconsistent ratios. For this reason, we interpret pre-treatment measurements in subsequent weeks as more reliable indicators of long-term O_3 impact, revealing the potential for recovery, which we explore in the next section.

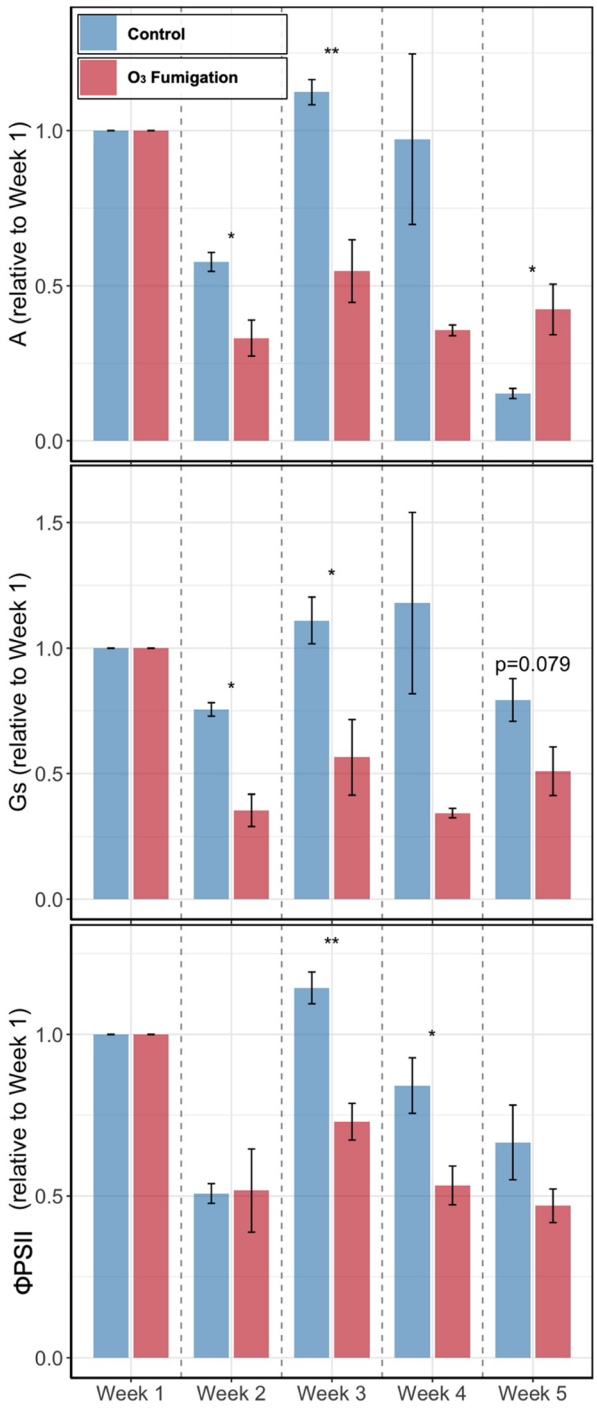

Fig. 5 Pre-treatment measurements of A (top), G_s (middle) and Φ_{PSII} (bottom) relative to week 1, in O_3-treated (red) and control (blue) soybean plants across five consecutive weeks. Bars are mean values ± SE ($n = 5$ leaves). Asterisks indicate significance levels (*$p < 0.05$, **$p < 0.01$).

3.2. O_3 exposure limits plants' ability to recover photosynthesis and efficiency

Focusing only on pre-treatment values allows us to assess how much plants recovered between exposures. Soybean plants showed limited resilience in photosynthetic function (Fig. 5). A brief decline in pre-treatment values observed in control plants in Week 2 likely reflects short-term acclimation to handling and repeated chamber placement; control plants subsequently stabilized or increased physiological parameters, indicating recovery and continued development under constant growth conditions. After the first fumigation, A and G_s never fully returned to pre-fumigation levels in O_3-treated plants – in clear contrast to control plants, which maintained stable or increasing values across the same period. Similarly, Φ_{PSII} declined and remained suppressed in fumigated plants, as opposed to controls. This trend indicates that O_3 not only limits carbon assimilation and gas exchange, but also impairs photochemical efficiency, further constraining recovery potential. Thus, while the impact of the first O_3 treatment may not have been extreme relative to the control on immediate, post-treatment parameters, plant damage was clear within a week, reflecting interrupted development from the modest four-hour O_3 fumigation at 80 ppb. Thus, O_3 exposure not only causes an immediate – albeit subtle – stress on the time scale of hours, but also causes a longer-term response of suppressed growth on the time scale of days to weeks. These findings align with other controlled studies showing that repeated O_3 exposures compromise recovery processes such as stomatal reopening and enzymatic function in the Calvin cycle.[9,23] Suppression of Φ_{PSII} is consistent with reports of O_3-induced damage at the chloroplast level,[22] as well as with declines in canopy-scale fluorescence under elevated O_3.[26]

Pre-treatment measurements show that O_3-treated plants failed to recover photosynthetic function between exposures, with sustained suppression of A, G_s, and Φ_{PSII} indicating an ongoing physiological burden that extends beyond short-term inhibition and is reflected in the slower growth patterns described in the following section.

3.3. Subtle O_3 exposure suppresses soybean growth and biomass

O_3 exposure impacted morphological development. Weekly measurements showed stalk height increasing more slowly in O_3-treated plants than in control plants (Fig. 6). By the end of the five-week experiment, average plant height in the fumigated group was consistently lower, even though no visible foliar damage was apparent. Final dry weight (DW) measurements supported this pattern, with non-fumigated plants accumulating more biomass (0.26 ± 0.04 g DW) than fumigated plants (0.21 ± 0.03 g DW). This growth suppression under ambient O_3 aligns with prior findings that O_3 reduces biomass accumulation even in the absence of necrotic symptoms.[9] This effect is likely caused by reduced carbon uptake due to the observed lower assimilation rates (see Section 3.2), combined with a shift in resource allocation from growth processes to antioxidant defense mechanisms.[23]

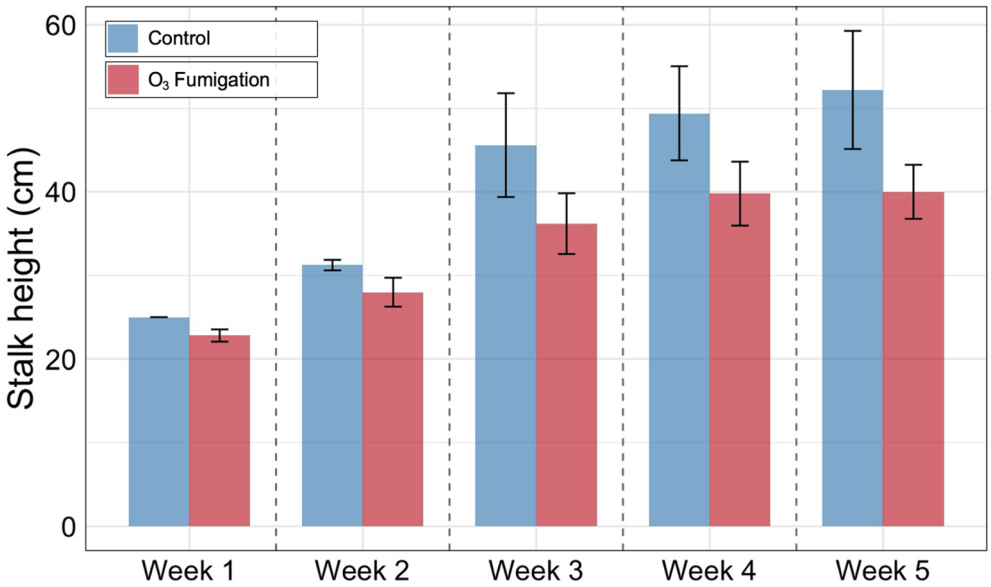

Fig. 6 Weekly stalk height measurements of soybean plants under O_3 fumigation (red) and control conditions (blue) over a five-week period. Bars represent mean stalk height ± SE (n = 5 stalks).

The impact of fumigation on growth persisted despite some recovery of gas exchange parameters in later weeks (see Section 3.2), suggesting that the effect of O_3 on developmental processes extends beyond short-term photosynthetic inhibition. This reinforces the concept that chronic, sub-lethal O_3 exposure slows physiological development, especially when plants are exposed early in their growth cycle. These results are consistent with SoyFACE observations, where long-term O_3 exposure reduced canopy height and biomass even when visual damage was absent.[25,26] However, our results further demonstrate that even more subtle and occasional changes in O_3, consistent with realistic scenarios currently occurring in agricultural regions, are sufficient to suppress plant growth and reduce biomass.

3.4. Long-term O_3 exposure decouples photosynthetic efficiency from fluorescence signals

Further analysis of pre-treatment values, discussed in Section 3.2, revealed that a relationship between Φ_{PSII} and its fluorescence components (F_m' and F_s) weakened and differed between treatments under repeated O_3 exposure (Fig. 7). Because Φ_{PSII} is

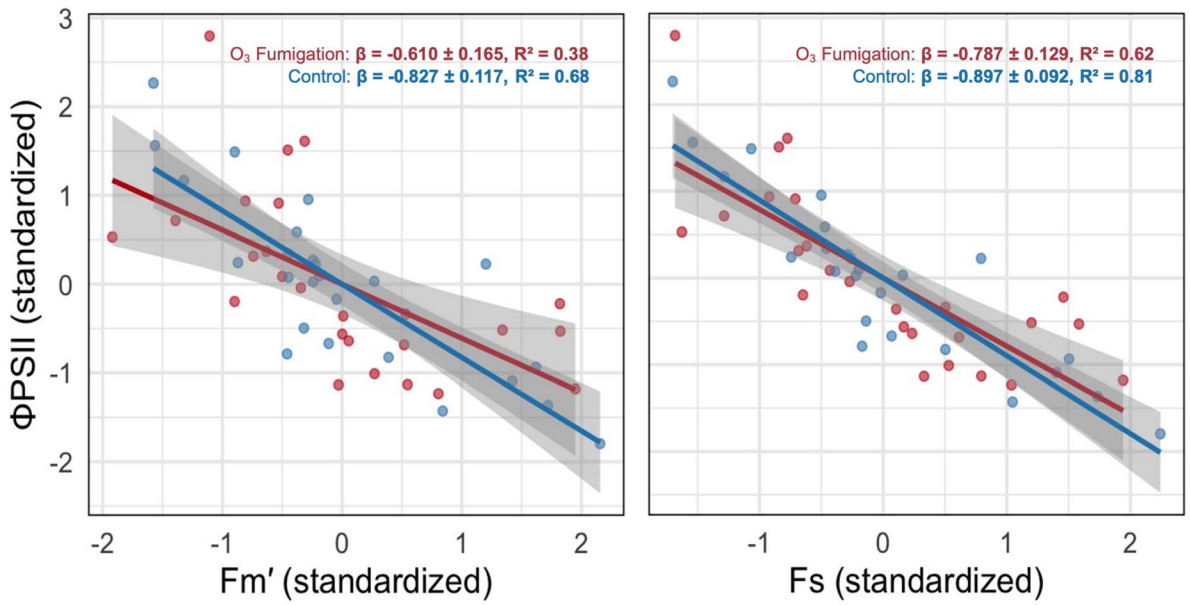

Fig. 7 Relationships between Φ_{PSII} and fluorescence components (F_m' – left, and F_s – right) under O_3 fumigation (red) and control conditions (blue) presented by pre-treatment measurements across five weeks. Slopes (β ± SE) and R^2 are shown for each treatment; p-values < 0.001.

calculated as $(F_m' - F_s)/F_m'$, these variables are not independent and nonlinear behavior is expected; however, the treatment-dependent reduction in explained variance and altered fitted relationships suggests increased variability in fluorescence-efficiency coupling under O_3 stress. Φ_{PSII} is usually tightly linked to its fluorescence components, reflecting a balance between absorbed light energy, photochemistry, and non-photochemical quenching.[46]

Observed decoupling indicates an imbalance between electron transport and energy dissipation, characteristic of strain-phase stress responses,[20] which implies that plants under chronic O_3 exposure may dissipate light energy in ways that no longer track with photochemical efficiency, an early-warning signal of impaired photosynthetic regulation.[47] Furthermore, Betzelberger *et al.*[8] argue that Φ_{PSII} is among the most sensitive fluorescence-derived parameters to O_3 stress in soybean, even when gas exchange traits partially recover and that indices based solely on F_s may fail to detect strain, highlighting why Φ_{PSII} offers a more mechanistic indicator of early stress.

Note that discussed decoupling was not observed in immediate post-treatment measurements, where F_m' and F_s maintained similar slopes and R^2 with Φ_{PSII} for fumigated and non-fumigated plants (Fig. S5). This close relationship reinforces the idea, emphasized in previous sections, that the impact of O_3 is not immediately visible after exposure, but emerges over longer timescales and disrupts the functional link between fluorescence signals and Φ_{PSII} efficiency.

4. Remote sensing analysis

4.1. Effect of first O_3 episode in the growing season is more visible than equivalent exposure later

To test whether the timing of O_3 stress modulates crop responses, we identified O_3 episodes as weeks when AOT40 increased by more than 350 ppb h relative to the previous week. This threshold was selected to capture episodic O_3 anomalies above local background conditions that occur regularly in the study region. For each of the four growing seasons (2018–2021), the earliest such episode was paired with a later episode of equivalent magnitude within the same season ($n = 4$, Table S1). To minimize influence of other environmental variables, the later episode was chosen to match the first one to have similar PAR, WB, RH, VPD, and T_{max} values. Remote sensing vegetation indicators are shown as absolute weekly values (units given in Table 1) and are compared across first *versus* later O_3 episodes (Fig. 8). Here, a negative effect is defined as a reduction in vegetation indicators during the first seasonal O_3 episode relative to a later episode of equivalent O_3 magnitude (ΔAOT40 > 350 ppb h) within the same growing season, rather than relative to an absolute ambient O_3 baseline. Another approach to minimizing seasonality trends was residualizing vegetation

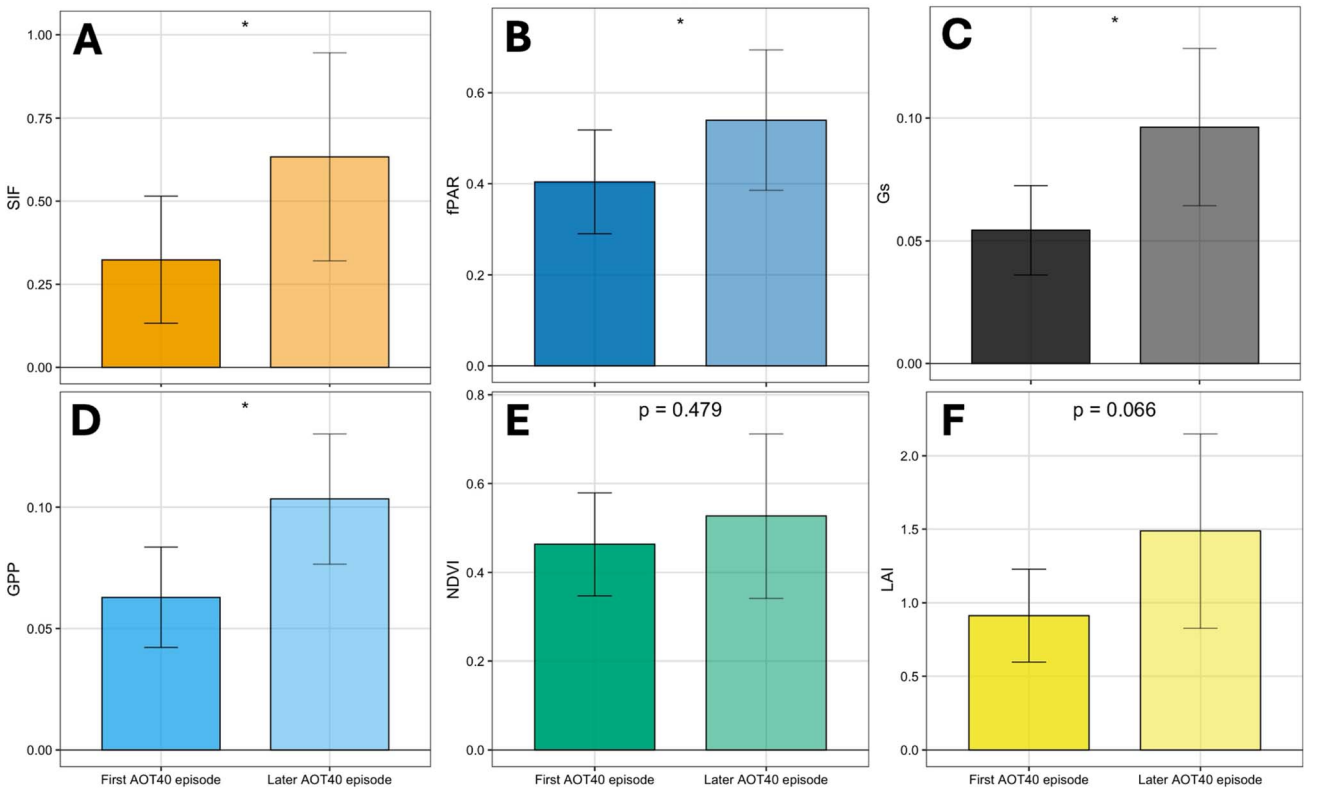

Fig. 8 Vegetation health indicators values compared between the first and later O_3 episodes of equivalent AOT40 increase (>350 ppb h) within each growing season (2018–2021). Panels show (A) SIF, (B) fPAR, (C) G_s, (D) GPP, (E) NDVI, and (F) LAI. Bars represent absolute mean weekly values of each indicator (units as in Table 1) ± SE across four paired episodes; no baseline normalization or temporal smoothing beyond weekly aggregation was applied. Asterisks indicate significance levels (*$p < 0.05$).

indicators against same meteorological covariates; results from the two approaches were consistent (Fig. S6). Comparisons between early and later O_3 episodes in the remote sensing analysis are based on seasonal timing at the canopy scale and are not intended to imply direct phenological equivalence with the chamber experiment.

Across all four years, the first O_3 episode of the season had a significantly stronger negative impact on functional indicators compared to equivalent exposures later in the season. SIF, GPP, fPAR, and G_s all showed significantly lower values during early-season episodes, while NDVI and LAI, which follow structural canopy development were not significantly different between two episodes. Notably, in 2020 and 2021 the first major O_3 episodes occurred later within the early growing period (Table S1), yet the relative suppression during first *versus* later episodes was comparable to that observed in 2018 and 2019, suggesting that the response is not solely driven by absolute seasonal timing. These findings mirror the leaf-level results (Section 3.1), where the first O_3 fumigation caused the largest drop in A and G_s, while following exposures triggered more muted responses as plants initiated partial defense mechanisms. Together, our results emphasize that the soybean is particularly vulnerable to O_3 early in its vegetative cycle, when photosynthetic capacity and resource allocation patterns are still being established.[8]

Physiologically, early vulnerability could be the result of the rapid development of sink capacity, which promotes O_3 uptake and amplifies oxidative stress.[9,21] At this stage, antioxidant defenses and photoprotective processes have not yet fully developed, leaving Φ_{PSII} particularly vulnerable to disruption.[22,23] This seasonal sensitivity is consistent with FACE experiments, in which chronic O_3 exposure accelerated senescence and reduced photosynthetic capacity, particularly during reproductive development.[25,26] Our results extend these insights by demonstrating that short-term, episodic O_3 events, found in agricultural regions – well below regulatory thresholds and chronic FACE exposures – can induce measurable strain when they occur early in the season. The strong suppression of SIF (A) and GPP (D) during these episodes underscores their value as functional indicators for detecting O_3 stress before visible canopy changes occur (E and F), in line with regional studies reporting stronger SIF–O_3 coupling during early vegetative stages.[16,17]

4.2. Real-world O_3 episodes slow down plant recovery

Using the O_3 episodes identified in Section 4.1 (ΔAOT40 > 350 ppb h), we observe how soybean vegetation health indicators recover from their first seasonal O_3 event compared to a later event (Fig. 9). Recovery trajectories are based on absolute weekly values of vegetation indicators following identified O_3 episodes, without normalization to a baseline. We are aware that values of our vegetation indices could in principle be influenced by differences in canopy development between early and later episodes. However, as shown in Section 4.1, structural parameters such as NDVI and LAI did not differ significantly between the paired events, suggesting that canopy development was not a major confounding factor.

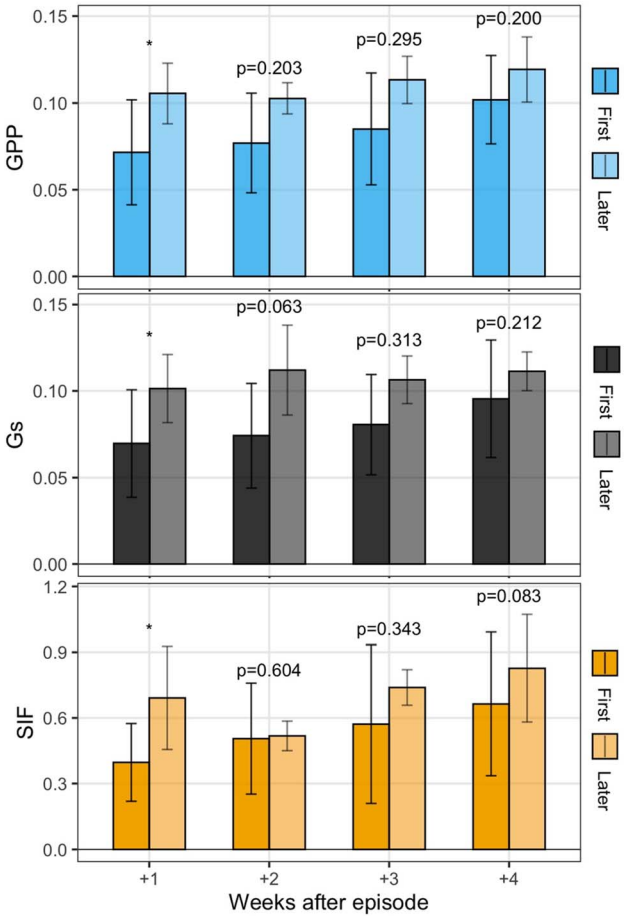

Fig. 9 Recovery of functional vegetation indicators (GPP, G_s, and SIF) following the first (dark bars) *vs.* later (light bars) seasonal O_3 episodes (ΔAOT40 > 350 ppb h). Bars show absolute mean weekly values of each indicator (units as in Table 1) ± SE across four growing seasons (2018–2021); no baseline normalization or temporal smoothing beyond weekly aggregation was applied. Asterisks indicate significance levels (*p < 0.05).

Results show that functional indicators (GPP, G_s, and SIF) were consistently more suppressed in the week following the first seasonal O_3 episode, compared to later episodes. In subsequent weeks, the gap between early and later episodes narrowed, suggesting canopy-scale recovery. This recovery contrasts with the chamber experiment (Section 3.2), where fumigated plants failed to recover fully between weekly exposures. The consistent stability of GPP, G_s, and SIF after later-season O_3 episodes suggests that plants may adapt to previously experienced strain. Structural indicators such as LAI, fPAR, and APAR (Fig. S7) showed similar patterns – significant suppression after early episodes followed by recovery. Notably, LAI indicates that canopy development slowed after the first O_3 episode, compared to later ones, consistent with chamber findings on growth suppression (Section 3.3).

The multi-week recovery lag observed after early episodes aligns with leaf-level evidence from Section 3.2. As the season progresses, acclimation and phenological shifts likely shorten this lag by increasing sink strength, enhancing antioxidant

defences, and adjusting stomatal sensitivity, buffering transient O_3 pulses.[8,16,23] These processes, and acclimation to an earlier strain phase,[20] may explain the reduced sensitivity to later O_3 episodes.

4.3. Higher O_3 accumulation in early and peak growing season reduces final soybean yield

We used cumulative GPP as a proxy for soybean yield[48–50] to examine how seasonal accumulations of AOT40 translate into productivity losses (Fig. 10). Results show that total accumulated O_3 across the full season did not correlate with yield ($R^2 = 0.04$, $p = 0.81$). Instead, exposure during the early growing season alone explained 47% of variance in cumulative GPP, and when early and peak seasons were combined, the relationship strengthened dramatically ($R^2 = 0.98$, $p = 0.01$). The strong predictive power of early and peak season exposure for final yield also aligns with meta-analyses showing that reproductive and vegetative transitions are the most sensitive phases for soybean yield determination[16,17] Given the limited and small number of seasons observed, these cumulative relationships are interpreted as descriptive associations that motivate the within-season analyses, rather than as causal attribution of yield responses to O_3 alone.

This finding reinforces our plant-level results (Section 3.3), where growth suppression occurred even in the absence of visible foliar damage. Furthermore, we connect findings from Sections 3.1 and 4.1, which showed that early-season exposures leave lasting impacts while later episodes have weaker effects, highlighting that it is not the total seasonal O_3 dose that determines yield losses, but rather when an elevated exposure event occurs. Early and peak stages, when plants are expanding canopies and establishing reproductive sinks, are the most consequential for O_3 impacts.[9,25]

For real-world application, we show that monitoring and mitigating O_3 during the early and peak growing season is critical for protecting yields, shedding light on potential mechanisms behind regional yield losses reported in the U.S. and Asia, where seasonal O_3 episodes often cluster in late spring and early summer.[18,19] Early strain detection using SIF and other functional indicators, as demonstrated in previous sections, could allow agronomists and farmers to take adaptive actions before the damage phase occurs and losses become irreversible. The seasonal distribution of O_3 further supports this conclusion. For example, 2019 had the highest total accumulated AOT40 but yielded relatively well because much of the exposure occurred late in the season (Fig. S8). By contrast, the high combined early and peak season exposure of 2018 had the lowest yield. These results emphasize that policies and crop management strategies must consider seasonal timing of O_3 exposure, not just seasonal totals or regulatory exceedances.

4.4. Accumulated O_3 affects relationships between remote sensing vegetation health indicators

We split the early and peak dataset into AOT40 tertiles (≤311, 311–508, ≥508 ppb h), comprising $n = 26$, 22, and 25 weekly observations, respectively, and within each class fit standardized regressions. We define these tertiles as 'lower', 'middle', and 'higher' O_3 exposure. Relationships between GPP-SIF, Gs-SIF, LAI-SIF, fPAR-GPP, and fPAR-SIF, stayed statistically strong across all classes (Fig. S9); the main changes were modest shifts in explained variance rather than large slope breaks. The fact that all of the relationships remained significant across classes suggests that basic canopy coordination is maintained, even if stress reduces its strength. Accordingly, changes in coupling are interpreted as O_3-associated patterns under realistic meteorological covariance, rather than as O_3-only effects.

Moving beyond GPP–SIF–fPAR–G_s relationships, we also examined how O_3 alters broader coordination between light absorption, fluorescence, and efficiency. Fig. 11 shows six additional relationships (APAR–GPP, APAR–SIF, LUE–G_s, LUE–SIF, SIFyield–G_s, and SIFyield–LUE) across AOT40 tertiles. These

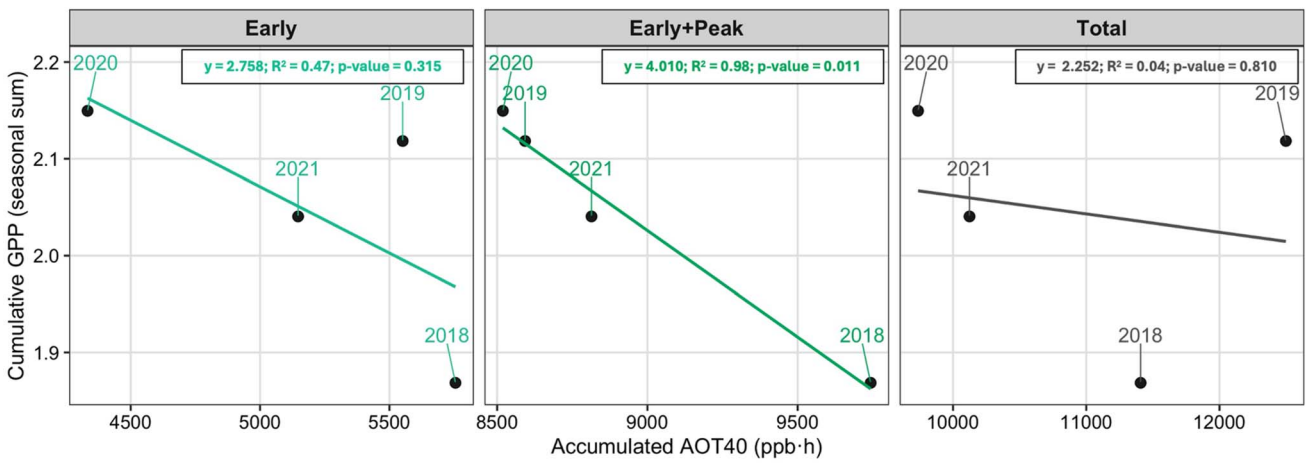

Fig. 10 Seasonal cumulative GPP as a proxy for soybean yield plotted against accumulated AOT40 (ppb h). Panels show relationships for early season only (left), early + peak seasons (middle), and the total growing season (right). Lines indicate linear regression fits with corresponding R^2 and p-values.

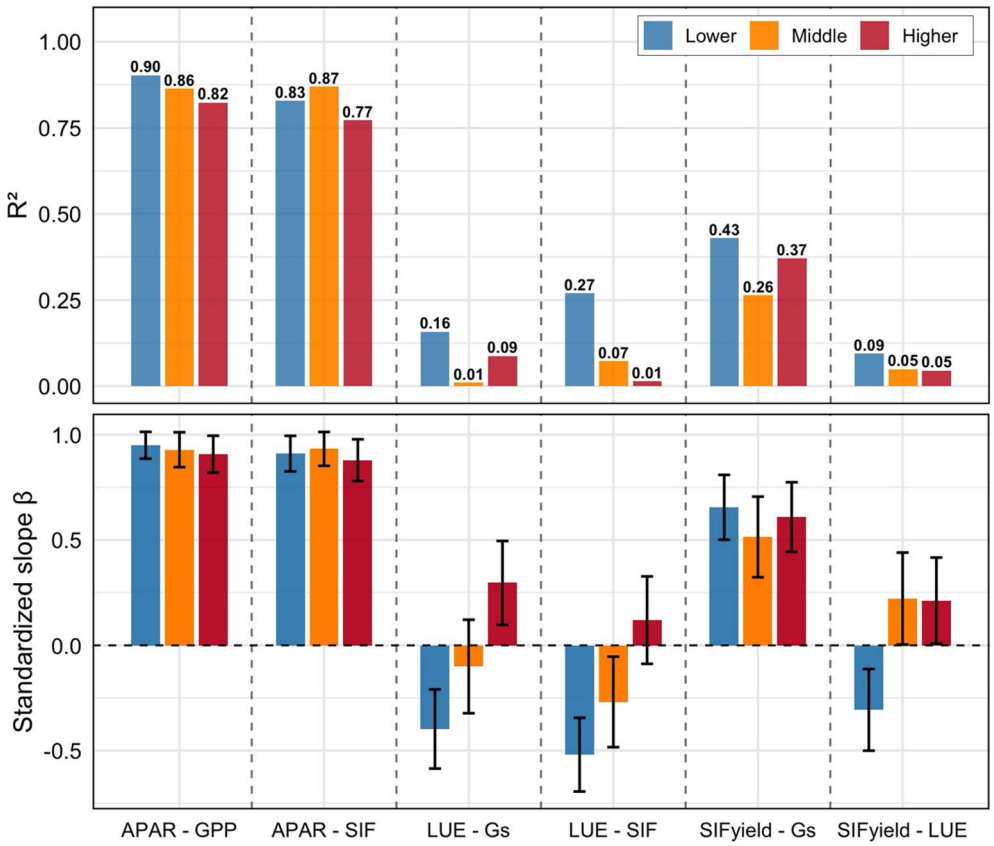

Fig. 11 Relationships between vegetation health indicators during the early and peak soybean growing season by different O_3 exposure. Bars show standardized regression slopes (β, bottom) ± SE, and coefficients of determination (R^2, top) for pairs of functional and structural indicators. Lower (blue), middle (orange), and higher (red) tertiles correspond to AOT40 thresholds of ≤311, 311–508, and ≥508 ppb h and include $n = 26$, 22, and 25 weekly observations, respectively.

metrics explicitly link absorbed energy, stomatal control, and realized carbon gain, and therefore allow us to assess whether O_3 disrupts not just single pairings but the broader chain of processes from light capture to photosynthesis.

Relationships linking absorbed light to productivity (APAR–GPP) and fluorescence (APAR–SIF) remained strong across all classes but weakened under high O_3 which indicates that while canopies continued absorbing and re-emitting light, their ability to convert light into carbon gain declined, reflecting reduced LUE.[8,23] Similarly, the already weak LUE–G_s relationship eroded with higher O_3, consistent with additional biochemical limitations beyond stomatal control.[5]

Relationships between efficiency metrics collapsed at high O_3. The LUE–SIF correlation, low, but present under lower exposures, disappeared in the highest class, suggesting that fluorescence no longer tracks photosynthetic efficiency under O_3 stress. This canopy-scale pattern mirrors the leaf-level decoupling observed between Φ_{PSII} and F_m'/F_s in Section 3.4, reinforcing that O_3 disrupts the coherence between photochemical signals and productivity across scales.[51] On the other hand, SIFyield–LUE was almost zero under all O_3 classes, indicating a full decoupling between fluorescence efficiency and realized carbon gain.

Intermediate relationships, such as SIFyield–G_s, also weakened with rising O_3, suggesting that stomatal regulation of fluorescence efficiency is partly maintained but insufficient to buffer stress. These findings highlight that accumulated O_3 not only weakens individual linkages but also fragments the entire chain from absorbed light → stomata → fluorescence → carbon gain.

By comparing these canopy-scale patterns with chamber experiments, we see consistent evidence that O_3 drives a progressive decoupling of functional indicators. While chambers revealed leaf-level strain through impaired Φ_{PSII} relationships, the remote sensing analysis demonstrates that the same disruption propagates across multiple efficiency metrics at the regional scale. This underscores the value of SIF and derived quantities like SIFyield for identifying when stress pushes canopies from coordinated functioning into a decoupled strain phase.

A sensitivity analysis refitting the within-tertile regressions with meteorological covariates (Fig. S10 and S11) shows that while some relationships remain similar, others change in magnitude and, in some cases, strengthen at higher O_3 exposure, indicating non-monotonic responses and changes in functional coupling. We emphasize that although this sensitivity analysis is useful for accounting for key meteorological covariates, it may also mask aspects of O_3 influence, as O_3 is never isolated from meteorology in real-world systems. For this reason, we do not attribute the observed relationships solely to

O_3; instead, the tertile-based approach is used to capture changes and non-linear patterns across increasing O_3 levels, rather than relying on a binary or fully detrended framework.

5. Conclusions

This study links leaf-level chamber experiments with regional satellite observations to advance mechanistic understanding of how O_3 affects soybean physiology under realistic exposure conditions. Across both scales, we find that the timing of O_3 stress is more important than its cumulative dose. In chambers, the first fumigation event caused the strongest suppression of photosynthesis (A and G_s) and efficiency (Φ_{PSII}), initiating a strain phase from which plants did not fully recover. Recovery between weekly exposures was incomplete, leading to sustained growth suppression – despite the quite moderate levels of air pollution used herein. A limitation of the plant-level experiment is the small number of samples per treatment, which may limit statistical power and generalizability. However, the purpose of this experiment is to elucidate mechanistic responses to episodic O_3 exposure that can be evaluated and contextualized using independent regional-scale remote sensing observations. Accordingly, chamber and satellite analyses are linked through shared response mechanisms (*e.g.*, strain-phase behavior and recovery limitations) rather than through direct alignment of phenological stages.

The controlled chamber experiments applied repeated exposures to mildly elevated O_3, consistent with conditions typical of North American agroecosystems. We note that fumigation levels were below the thresholds set by the U.S. EPA for human health. The National Ambient Air Quality Standard is based on an 8 hours average of 70 ppb, while we show that exposures equivalent to a weekly 8 hours average of 40 ppb, or a 4 hours average of 80 ppb, were sufficient to cause significant stress and clear reductions in crop productivity. Our findings highlight the need for regulators to consider agricultural impacts when managing O_3 precursors, which is particularly urgent given that wildfire smoke, rising temperatures, and other climate-related drivers are likely to increase regional O_3 episodes in the future.[52,53]

At the regional scale, multi-year satellite observations confirmed that early-season O_3 episodes produced stronger declines in SIF, GPP, and G_s than equivalent late-season exposures, with recovery lagging for several weeks. Seasonal yield proxies were best explained not by total O_3 accumulation, but instead by exposures during early and peak growth phases, when canopies are expanding and reproductive sinks are being established. At this scale, O_3 effects are evaluated under realistic environmental covariance, and results highlight changes in functional coordination rather than O_3-only attribution. These findings bridge controlled and field conditions, demonstrating that even subtle, episodic O_3 events can constrain soybean productivity when they occur at vulnerable stages – highlighting the potential of functional indicators such as SIF to detect stress before irreversible damage occurs.

A limitation of this study is the coarse resolution of the TROPOMI SIF product (~7 × 3.5 km), which restricts application to small fields. Nevertheless, the physiological mechanisms identified, and detection strategies developed herein, are broadly transferable across agricultural systems. The upcoming ESA FLEX mission, dedicated to fluorescence monitoring at finer spatial scales, carries potential to enhance the applicability of these approaches, enabling earlier and more precise detection of O_3 stress. Additionally, while stricter regulation of O_3 precursors in agricultural regions could help protect crop productivity, such measures are difficult to implement as high O_3 events often coincide with heat waves and drought, which themselves increase precursor emissions. We therefore emphasize the need to reduce ground-level O_3 as part of integrated strategies for crop health and global food security in a changing climate.

Conflicts of interest

There are no conflicts to declare.

Data availability

All data supporting the findings of this study are available within the article and its supplementary information (SI). Chamber experiment data and processed remote sensing datasets used in this study are available from the corresponding author upon reasonable request. Satellite remote sensing datasets are publicly accessible from ESA-TROPOSIF (SIF), MODIS (NDVI, LAI, fPAR, GPP), and GRIDMET (meteorology). Ground-level O_3 observations were obtained from the U.S. Environmental Protection Agency (EPA) Air Quality System (AQS). Supplementary information is available. See DOI: https://doi.org/10.1039/d5em00785b.

Acknowledgements

This paper and related research have been conducted within the framework of the Italian National PhD Program in Earth Observation funded by the European Union – Next Generation EU through the Project of Italian Recovery and Resilience Plan (NRRP) (B53C22004370006). The TROPOSIF products were generated by the TROPOSIF team conducted by NOVELTIS under the European Space Agency (ESA) Sentinel-5p+ Innovation activity Contract No. 4000127461/19/I-NS. We acknowledge funding from a National Science Foundation AGS Postdoctoral Research Fellowship (MR; 2306215). We would like to acknowledge the help of Lydia Tonnesen and Alyssa Belanger, who assisted with planting and caring for our soybean plants throughout the entire plant-level experiment. We thank the three anonymous reviewers for their comments, which helped improve this manuscript.

References

1 D. Dong and J. Wang, Air pollution as a substantial threat to the improvement of agricultural total factor productivity: Global evidence, *Environ. Int.*, 2023, **173**, 107842.

2 A. P. K. Tai, M. V. Martin and C. L. Heald, Threat to future global food security from climate change and ozone air pollution, *Nat. Clim. Change*, 2014, **4**(9), 817–9821.
3 M. R. Ashmore, Assessing the future global impacts of ozone on vegetation, *Plant Cell Environ.*, 2005, **28**(8), 949–964, DOI: 10.1111/j.1365-3040.2005.01341.x.
4 L. D. Emberson, P. Büker, M. R. Ashmore, G. Mills, L. S. Jackson, M. Agrawal, *et al.*, A comparison of North American and Asian exposure–response data for ozone effects on crop yields, *Atmos. Environ.*, 2009, **43**(12), 1945–1953.
5 O. E. Clifton, A. M. Fiore, W. J. Massman, C. B. Baublitz, M. Coyle, and L. Emberson, *et al.*, Dry Deposition of Ozone Over Land: Processes, Measurement, and Modeling, in *Reviews of Geophysics*, Blackwell Publishing Ltd, vol. 58, 2020.
6 S. Fares, F. Savi, J. Muller, G. Matteucci and E. Paoletti, Simultaneous measurements of above and below canopy ozone fluxes help partitioning ozone deposition between its various sinks in a Mediterranean Oak Forest, *Agric. For. Meteorol.*, 2014, **198–199**, 181–191.
7 G. Mills, H. Pleijel, C. S. Malley, B. Sinha, O. R. Cooper, M. G. Schultz, *et al.*, Tropospheric ozone assessment report: Present-day tropospheric ozone distribution and trends relevant to vegetation, *Elementa*, 2018, **6**, 47.
8 A. M. Betzelberger, C. R. Yendrek, J. Sun, C. P. Leisner, R. L. Nelson, D. R. Ort, *et al.*, Ozone exposure response for U.S. soybean cultivars: Linear reductions in photosynthetic potential, biomass, and yield, *Plant Physiol.*, 2012, **160**(4), 1827–1839.
9 P. B. Morgan, E. A. Ainsworth and S. P. Long, How does elevated ozone impact soybean? A meta-analysis of photosynthesis, growth and yield, *Plant Cell Environ.*, 2003, **26**(8), 1317–1328.
10 Z. Feng, E. Hu, X. Wang, L. Jiang and X. Liu, Ground-level O3 pollution and its impacts on food crops in China: A review, *Environ. Pollut.*, 2015, **199**, 42–48.
11 E. A. Ainsworth, Understanding and improving global crop response to ozone pollution, *Plant J.*, 2017, **90**(5), 886–897.
12 G. Mills, K. Sharps, D. Simpson, H. Pleijel, M. Broberg, J. Uddling, *et al.*, Ozone pollution will compromise efforts to increase global wheat production, *Glob. Change Biol.*, 2018, **24**(8), 3560–3574.
13 A. Y. H. Wong, J. A. Geddes, J. A. Ducker, C. D. Holmes, S. Fares, A. H. Goldstein, *et al.*, New Evidence for the Importance of Non-Stomatal Pathways in Ozone Deposition During Extreme Heat and Dry Anomalies, *Geophys. Res. Lett.*, 2022, **49**(8), e2021GL095717.
14 J. M. McGrath, A. M. Betzelberger, S. Wang, E. Shook, X. G. Zhu, S. P. Long, *et al.*, An analysis of ozone damage to historical maize and soybean yields in the United States, *Proc. Natl. Acad. Sci. U. S. A.*, 2015, **112**(46), 14390–14395.
15 B. S. Felzer, T. Cronin, J. M. Reilly, J. M. Melillo and X. Wang, Impacts of ozone on trees and crops, *C. R. Geosci.*, 2007, **339**(11–12), 784–798.
16 C. M. Montes, H. J. Demler, S. Li, D. G. Martin and E. A. Ainsworth, Approaches to investigate crop responses to ozone pollution: from O3-FACE to satellite-enabled modeling, *Plant J.*, 2022, **109**(2), 432–446, DOI: 10.1111/tpj.15501.
17 Z. Feng and K. Kobayashi, Assessing the impacts of current and future concentrations of surface ozone on crop yield with meta-analysis, *Atmos. Environ.*, 2009, **43**(8), 1510–1519.
18 A. P. K. Tai, M. Sadiq, J. Y. S. Pang, D. H. Y. Yung and Z. Feng, Impacts of Surface Ozone Pollution on Global Crop Yields: Comparing Different Ozone Exposure Metrics and Incorporating Co-effects of CO2, *Front. Sustain. Food Syst.*, 2021, **5**, 534616.
19 F. Leung, S. Sitch, A. P. K. Tai, A. J. Wiltshire, J. L. Gornall, G. A. Folberth, *et al.*, CO2 fertilization of crops offsets yield losses due to future surface ozone damage and climate change, *Environ. Res. Lett.*, 2022, **17**(7), 074007.
20 M. Meroni, C. Panigada, M. Rossini, V. Picchi, S. Cogliati and R. Colombo, Using optical remote sensing techniques to track the development of ozone-induced stress, *Environ. Pollut.*, 2009, **157**(5), 1413–1420.
21 E. Singh, S. Tiwari and M. Agrawal, Effects of elevated ozone on photosynthesis and stomatal conductance of two soybean varieties: A case study to assess impacts of one component of predicted global climate change, *Plant Biol.*, 2009, **11**(suppl.1), 101–108.
22 C. P. Chen, T. D. Frank and S. P. Long, Is a short, sharp shock equivalent to long-term punishment? Contrasting the spatial pattern of acute and chronic ozone damage to soybean leaves via chlorophyll fluorescence imaging, *Plant Cell Environ.*, 2009, **32**(4), 327–335.
23 S. A. Osborne, G. Mills, F. Hayes, E. A. Ainsworth, P. Büker and L. Emberson, Has the sensitivity of soybean cultivars to ozone pollution increased with time? An analysis of published dose-response data, *Glob. Change Biol.*, 2016, **22**(9), 3097–3111.
24 S. C. Kavassalis and J. G. Murphy, Understanding ozone-meteorology correlations: A role for dry deposition, *Geophys. Res. Lett.*, 2017, **44**(6), 2922–2931.
25 E. A. Ainsworth, S. P. Serbin, J. A. Skoneczka and P. A. Townsend, Using leaf optical properties to detect ozone effects on foliar biochemistry, *Photosynth. Res.*, 2014, **119**(1–2), 65–76.
26 G. Wu, K. Guan, E. A. Ainsworth, D. G. Martin, H. Kimm and X. Yang, Solar-induced chlorophyll fluorescence captures the effects of elevated ozone on canopy structure and acceleration of senescence in soybean, *J. Exp. Bot.*, 2024, **75**(1), 350–363.
27 D. M. Eastburn, M. M. Degennaro, E. H. Delucia, O. Dermody and A. J. Mcelrone, Elevated atmospheric carbon dioxide and ozone alter soybean diseases at SoyFACE, *Glob. Change Biol.*, 2010, **16**(1), 320–330.
28 X. Liu and A. R. Desai, Significant Reductions in Crop Yields From Air Pollution and Heat Stress in the United States, *Earths Future*, 2021, **9**(8), e2021EF002000, DOI: 10.1029/2021EF002000.
29 O. R. Cooper, K. L. Chang, K. Bates, S. S. Brown, W. S. Chace, M. M. Coggon, *et al.*, Early Season 2023 Wildfires Generated Record-Breaking Surface Ozone Anomalies Across the U.S.

Upper Midwest, *Geophys. Res. Lett.*, 2024, **51**(22), e2024GL111481, DOI: 10.1029/2024GL111481.
30 K. L. Chang, B. C. McDonald, C. Harkins and O. R. Cooper, Surface ozone trend variability across the United States and the impact of heat waves (1990–2023), *Atmos. Chem. Phys.*, 2025, **25**(10), 5101–5132.
31 A. K. Mahlein, E. C. Oerke, U. Steiner and H. W. Dehne, Recent advances in sensing plant diseases for precision crop protection, *Eur. J. Plant Pathol.*, 2012, **133**(1), 197–209, DOI: 10.1007/s10658-011-9878-z.
32 P. J. Pinter, J. L. Hatfield, J. S. Schepers, E. M. Barnes, M. S. Moran, C. S. T. Daughtry, *et al.*, Remote Sensing for Crop Management, *Photogramm. Eng. Rem. Sens.*, 2003, **69**(6), 647–664.
33 M. Riches, D. Lee and D. K. Farmer, Simultaneous leaf-level measurement of trace gas emissions and photosynthesis with a portable photosynthesis system, *Atmos. Meas. Tech.*, 2020, **13**(8), 4123–4139.
34 C. Julián, S. Villadangos, L. Jené, O. Pasques, M. Pintó-Marijuan and S. Munné-Bosch, Biological outliers: essential elements to understand the causes and consequences of reductions in maximum photochemical efficiency of PSII in plants, *Planta*, 2024, **260**(1), 32.
35 S. Alvarez Prado, I. Sanchez, L. Cabrera-Bosquet, A. Grau, C. Welcker, F. Tardieu, *et al.*, To clean or not to clean phenotypic datasets for outlier plants in genetic analyses?, *J. Exp. Bot.*, 2019, **70**(15), 3693.
36 C. Leys, C. Ley, O. Klein, P. Bernard and L. Licata, Detecting outliers: Do not use standard deviation around the mean, use absolute deviation around the median, *J. Exp. Soc. Psychol.*, 2013, **49**(4), 764–766.
37 J. Ross, *Arkansas Soybean Research Studies 2019*, Arkansas Agricultural Experiment Station Research Series, 2020, https://scholarworks.uark.edu/aaesser/166.
38 J. T. Abatzoglou, Development of gridded surface meteorological data for ecological applications and modelling, *Int. J. Climatol.*, 2013, **33**(1), 121–131, DOI: 10.1002/joc.3413.
39 N. P. Robinson, B. W. Allred, W. K. Smith, M. O. Jones, A. Moreno, T. A. Erickson, *et al.*, Terrestrial primary production for the conterminous United States derived from Landsat 30 m and MODIS 250 m, *Remote Sens. Ecol. Conserv.*, 2018, **4**(3), 264–280, DOI: 10.1002/rse2.74.
40 L. Guanter, C. Bacour, A. Schneider, I. Aben, T. A. Van Kempen, F. Maignan, *et al.*, The TROPOSIF global sun-induced fluorescence dataset from the Sentinel-5P TROPOMI mission, *Earth Syst. Sci. Data*, 2021, **13**(11), 5423–5440.
41 D. Wang, S. Liang, Y. Zhang, X. Gao, M. G. L. Brown and A. Jia, A New Set of MODIS Land Products (MCD18): Downward Shortwave Radiation and Photosynthetically Active Radiation, *Remote Sens.*, 2020, **12**(1), 168.
42 I. Lozano, I. Alados, G. Sánchez-Hernández, J. L. Guerrero-Rascado and I. Foyo-Moreno, Improving the Estimation of the Diffuse Component of Photosynthetically Active Radiation (PAR), *J. Geophys. Res. Atmos.*, 2023, **128**(22), e2023JD039256, DOI: 10.1029/2023JD039256.
43 T. S. Magney, D. R. Bowling, B. A. Logan, K. Grossmann, J. Stutz, P. D. Blanken, *et al.*, Mechanistic evidence for tracking the seasonality of photosynthesis with solar-induced fluorescence, *Proc. Natl. Acad. Sci.*, 2019, **116**(24), 11640–11645, DOI: 10.1073/pnas.1900278116.
44 G. Miao, K. Guan, X. Yang, C. J. Bernacchi, J. A. Berry, E. H. DeLucia, *et al.*, Sun-Induced Chlorophyll Fluorescence, Photosynthesis, and Light Use Efficiency of a Soybean Field from Seasonally Continuous Measurements, *J. Geophys. Res.:Biogeosci.*, 2018, **123**(2), 610–623, DOI: 10.1002/2017JG004180.
45 A. Massmann, P. Gentine and C. Lin, When Does Vapor Pressure Deficit Drive or Reduce Evapotranspiration?, *J. Adv. Model. Earth Syst.*, 2019, **11**(10), 3305–3320, DOI: 10.1029/2019MS001790.
46 K. Oxborough and N. R. Baker, Resolving chlorophyll a fluorescence images of photosynthetic efficiency into photochemical and non-photochemical components - Calculation of qP and Fv'/Fm' without measuring Fo', *Photosynth. Res.*, 1997, **54**(2), 135–142, DOI: 10.1023/A:1005936823310.
47 A. V. Ruban and E. H. Murchie, Assessing the photoprotective effectiveness of non-photochemical chlorophyll fluorescence quenching: A new approach, *Biochim. Biophys. Acta, Bioenerg.*, 2012, **1817**(7), 977–982.
48 P. M. Wurster, M. Maneta, J. S. Kimball, K. A. Endsley and S. Beguería, Monitoring Crop Status in the Continental United States Using the SMAP Level-4 Carbon Product, *Front. Big Data*, 2021, **3**, 597720.
49 C. Dold, J. L. Hatfield, J. H. Prueger, T. B. Moorman, T. J. Sauer, M. H. Cosh, *et al.*, Upscaling Gross Primary Production in Corn-Soybean Rotation Systems in the Midwest, *Remote Sens.*, 2019, **11**(14), 1688.
50 M. Marshall, K. Tu and J. Brown, Optimizing a remote sensing production efficiency model for macro-scale GPP and yield estimation in agroecosystems, *Remote Sens. Environ.*, 2018, **217**, 258–271.
51 J. Chen, S. Wang, K. Zhu, B. Chen, Q. Wang, L. Zhang, *et al.*, Tropospheric ozone alters solar-induced chlorophyll fluorescence and its relationship with gross primary production in a subtropical evergreen forest, *Agric. For. Meteorol.*, 2025, **372**, 110695.
52 L. Xu, J. D. Crounse, K. T. Vasquez, H. Allen, P. O. Wennberg, I. Bourgeois, *et al.*, Ozone chemistry in western U.S. wildfire plumes, *Sci. Adv.*, 2021, **7**(50), 3648.
53 S. E. Pusede, A. L. Steiner and R. C. Cohen, Temperature and Recent Trends in the Chemistry of Continental Surface Ozone, *Chem. Rev.*, 2015, **115**(10), 3898–3918, DOI: 10.1021/cr5006815.

